Dynamic Amplification of Drag Dominated Structures in Irregular Seas

Jan-Tore H. Horn
Centre for Autonomous
Marine Operations and Systems (AMOS)
Department of Marine Technology
Norwegian University of
Science and Technology
7491 Trondheim, Norway
Email: jan-tore.horn@ntnu.no

Jorgen Amdahl
Centre for Autonomous
Marine Operations and Systems (AMOS)
Department of Marine Technology
Norwegian University of
Science and Technology
7491 Trondheim, Norway
Email: jorgen.amdahl@ntnu.no

Sverre K. Haver
Department of Marine Technology
Norwegian University of
Science and Technology
7491 Trondheim, Norway
University of Stavanger, Norway
Email: sverre.k.haver@uis.no

***Abstract*—Offshore bottom-fixed structures, such as jackets, are typically designed with a natural period of 3 seconds or less. This means that there is limited dynamic excitation from wave loads at design sea-states. The benefit of this is reduced uncertainties from the dynamic effects in the design phase. However, some jacket structures in deep water or soft soil-conditions may have natural periods exceeding 4 seconds, which implies large dynamic effects. For a jack-up, industry guidelines are developed to account for the dynamic structural response in both ULS and FLS conditions. Although advanced methods are available to determine the dynamic amplification factors (DAF), they are unsuitable to estimate the dynamic response in the concept design phase. The current simplified method is based on a single-degree-of-freedom (SDOF) system. However, the estimator is not very accurate for the DAF of a structure in irregular seas, and must be used with caution. The most correct method for estimating the extreme static and dynamic responses is stochastic time-domain simulation. In this paper, it is investigated whether an analytical formulation is appropriate for DAF in irregular seas, as a function of natural period. The models used are a slender cylinder and a dynamically sensitive jacket, in an extreme sea-state. Non-linear quasi-static and dynamic time-domain analysis are carried out with USFOS, a computer program especially designed for space frame offshore structures, using linear wave theory and the Morison equation.**

I. Introduction

Subjecting the structure to a design wave can be an adequate approach to find the design loads at a certain probability level. This is usually done by stepping a Stoke 5^{th} wave through the structure. However, this is only recommended for structures with a low natural period (i.e. $< 2[s]$), where the dynamic effects are limited. Then, a DAF from an equivalent SDOF system can be multiplied with the quasi-static response. As the structures move to deeper water, the natural periods increase and more sophisticated methods are needed to account for dynamics. This has been done extensively in e.g. [1] for a dynamically sensitive jacket structure. For an increased natural period, non-linear effects causing a resonant response will be more prominent and thus causing large dynamic contributions to the DAF. For drag dominated structures the non-linear nature of the wave load will result in harmonic excitations at multiples of the load frequency, thus causing large dynamic responses for natural periods coinciding with these multiples. In [2], it is suggested to account for these super-harmonic excitations in the DAF estimator for SDOF systems subjected to multi-harmonic loads such as irregular waves. As we shall see, the wave elevation itself is a non-linearity that contributes to this behavior. The aim of this work is to get a better understanding of how the dynamic amplification varies with respect to the natural period.

However, when performing stochastic analysis, it is not expected that the extreme dynamic and quasi-static response will occur for the same incident wave. It is therefore more convenient to use an *equivalent* DAF (EDAF), which is used in [3]. This value is estimated based on the responses for a given probability of exceedance, which introduces some statistical uncertainties that will be addressed. All simulations in the time-domain have been performed using USFOS [4] computer software.

II. Simulation models and parameters

The time-domain analyses and statistical work have been performed on a slender cylinder and a jacket structure. The slender cylinder has a diameter of 1[m] and is located at 100[m] water depth. Its purpose is to demonstrate the response of a computationally efficient, drag dominated structure. The jacket is similar to the one used in [1] and [3]. The main

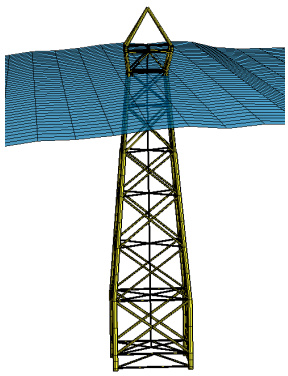

Fig. 1. Jacket computer model

specifications are given in Table I, and an illustration is shown in Fig. 1. The topside is replaced with a node mass at the topside center of gravity. Long crested waves are used, propagating with a heading of 45°, meaning that all braces are exposed to the wave kinematics.

TABLE I. JACKET

Legs	2.0-2.9 m
Braces	0.9-1.6 m
Depth	190 m

The structural damping is applied as Rayleigh damping with 1.3% at the first natural frequency and 1.5% at the third natural frequency. This is to assure a sufficiently low damping at the applied load period and natural period. Relative velocity is not used in calculation of drag forces, since it could overestimate the actual damping for small responses [5]. A time-step of 0.1[s] is applied in all simulations, and regarded as sufficient to capture dynamics in this case.

To find an appropriate ULS sea-state with an annual probability of 10^{-2}, the contourline method described in detail in [6] has been used. The assumption is that the long term extremes can be well estimated by a few short term extremes [7]. For conditions in the northern North Sea, a sea-state with T_P=16.3[s] and H_S=14.9[m], is identified as appropriate and will be used throughout the study. A JONSWAP spectrum is then applied with a cut-off frequency of $\omega_{cut} = 4\omega_P$, a peak shape parameter of 2.45 [8] and Rayleigh distributed random amplitudes [9]. For the hydrodynamic loading, USFOS uses the Morison equation with Wheeler stretching to the instantaneous water surface. Drag and mass coefficients are chosen according to [5], and are reproduced in Table II. They are larger than the standard coefficients in order to account for the underestimation made with Wheeler stretching in a Gaussian sea. Current is not accounted for in these analyses.

TABLE II. DRAG AND INERTIA COEFFICIENTS FOR FIRST ORDER SIMULATION

	$z < 2$ m	$z \geq 2$ m
C_D	1.15	1.15
C_M	1.2	1.6

III. BASIC PRINCIPLES

A. DAF

The analytical DAF for the SDOF system in Fig. 2 subjected to a harmonic force $f(t) = f_0 \exp(i\omega t)$, can be found by the dynamic and quasi-static equations of motion. These are given in eq. (1) and (2), respectively. Further, by assuming $x = x_0 \exp(i\omega t)$, we can solve for x_d and x_s and find the DAF in eq. (3). This equation is found in guidelines for assessment of jack-ups regarding dynamic amplification (see e.g. [10] and [11]).

$$\ddot{x}_d + 2\zeta\omega_n\dot{x}_d + \omega_n^2 x_d = \frac{1}{m}f(t) \tag{1}$$

$$\omega_n^2 x_s = \frac{1}{m}f(t) \tag{2}$$

where $\omega_n = \sqrt{k/m}$ is the undamped natural frequency.

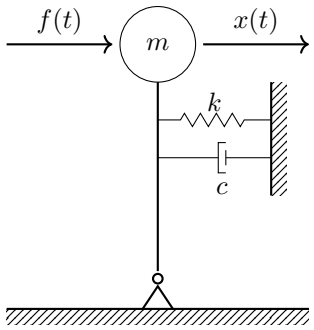

Fig. 2. SDOF system for small rotational displacements

$$DAF = \frac{x_d}{x_s} = \frac{1}{\sqrt{(1-\Omega^2)^2 + (2\zeta\Omega)^2}} \tag{3}$$

where $\Omega = \frac{\omega}{\omega_n} = \frac{T_n}{T}$, $T_n = \frac{2\pi}{\omega_n}$ is the natural period and T is the load period. To sum up, DAF, also referred to as dynamic load factor (DLF), can be interpreted as a transfer function from quasi-static to dynamic response.

B. EDAF

EDAF is defined as the q-probable dynamic response divided by the q-probable quasi-static response. That is, the response corresponding to an annual probability, q, of exceedance.

$$EDAF = \frac{X_{q,d}}{X_{q,s}} \tag{4}$$

If the long term response can be divided into short term stationary response records, each of a duration of 3 hours, the response can be found by solving

$$F_{X_{3h}}(X_q) = 1 - \frac{q}{365 \cdot 8} \tag{5}$$

requiring that the long term extreme response value is well approximated by $F_{X_{3h}}$. Here, the EDAF is estimated using a single design sea-state along the contourline corresponding to $q = 10^{-2}$. Meaning an assumption is made that this sea-state will provide the characteristic extremes for all sea-states satisfying $H_S = H_{S,q}$ and $T_P = T_{P,q}$. We can then obtain a distribution, $F_{X_{3h}|H_{S,q}T_{P,q}}(x|h_{s,q}t_{p,q})$, from a number of sample extremes from simulated response time series of length 3 hours. Finally, the approximate long term response, X_q, is found by

$$F_{X_{3h}|H_{S,q}T_{P,q}}(X_q|h_{s,q}t_{p,q}) = \alpha \tag{6}$$

where $\alpha = 0.9$ is a suitable fractile level given in [5].

C. Multi-harmonic DAF function

The multi-harmonic DAF function in eq. (7) given by [2], is simply a summation of frequency response functions for multiples of the non-dimensional eigenperiod, Ω.

$$\begin{aligned} DAF_{MH}(\Omega) &= \sum_{n=1}^{N} DAF_n(\Omega) \\ &= \sum_{n=1}^{N} \frac{k_n}{\sqrt{\left(1-(n\Omega)^2\right)^2 + \left(2(\zeta_n)n\Omega\right)^2}} \end{aligned} \tag{7}$$

The weight parameters k_n should satisfy $\sum k_n = 1$ and are decided based on the wave load spectrum. Larger weight factors means a broader peak. The individual damping parameters, ζ_n, represent total damping to match the extreme response for a given natural period. In other words, the damping ratios determine the height of the peaks. An example is given in Fig. 3, comparing the classical SDOF DAF analogy with the proposed function for some arbitrary parameters.

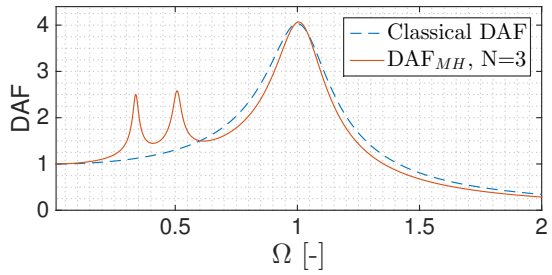

Fig. 3. Multi-harmonic DAF. $\bar{k} = [0.8, 0.1, 0.1]$, $\bar{\zeta} = [0.10, 0.03, 0.03]$.

IV. DAF in regular seas

A short study of the response in regular waves have been carried out to set a baseline before simulating random seas. For regular waves, a very short simulation time is needed after the transient phase (for dynamic analysis) to determine the steady-state harmonic peak responses.

A. Wave load

The wave load in regular seas can be obtained analytically with the Morison equation, also when multi-harmonic loading is accounted for. The drag term per unit length in the Morison equation reads:

$$f(t,z) = \frac{1}{2}\rho C_D D u(t,z)|u(t,z)| \tag{8}$$

where $u(t,z)$ is the normal particle velocity in x-direction. The equation is integrated over the element length, which depends on t and z. An analytical expression for the total load on a cylinder at water depth h[m] in sinusoidal waves with instantaneous elevation $\zeta(t)$[m] and Wheeler stretching can be expressed as:

$$\begin{aligned} F(t) &= \int_{-h}^{\zeta(t)} f(t,z)dz = c_1 f(t)\left[h+\zeta(t)\right] \\ &= \hat{c}_1 h \sin(\omega t)|\sin(\omega t)| + \hat{c}_1 \zeta_a \sin^2(\omega t)|\sin(\omega t)| \end{aligned} \tag{9}$$

where c_1 is an integration constant dependent on the wave number, k, and the depth. It can be shown that setting c_1=1 gives less than 10% error in eq. (9) when $\frac{2\pi}{\omega} > 18$[s] and h=100[m]. However, the constant is not of any importance as it does not change the relative values between the coefficients in eq. (10), where the expression is written as a Fourier series.

$$\begin{aligned} F_N(t) =& \hat{c}_1 \Big[C_1 \sin(\omega t) + C_2 \cos(2\omega t) + C_3 \sin(3\omega t) \\ &+ C_4 \cos(4\omega t) + C_5 \sin(5\omega t) + ...\Big] \end{aligned} \tag{10}$$

where the coefficients are given in Table III. The procedure is similar to what is done in [12].

TABLE III. Fourier coefficients

C_1	C_2	C_3	C_4	C_5
$\frac{8}{3\pi}h$	$-\frac{8}{5\pi}\zeta_a$	$-\frac{8}{15\pi}h$	$\frac{8}{35\pi}\zeta_a$	$-\frac{8}{105\pi}h$

From the Fourier series, it is obvious that the load will excite with frequencies $n\omega$ for $n = 1, 2, 3....$ The relative contribution from each term will depend on the wave amplitude and water depth. In short, C_1, C_3 and C_5 are due to the non-linear drag loading which has several harmonics, while C_2 and C_4 are due to the integration to the instantaneous surface. The spectral density of the wave load is presented in Fig. 4 for the present case, where $\frac{\zeta_a}{h} = 0.075$. Note that the inertia force has small peaks at $\frac{\omega}{\omega_R} = 2, 3, ...$ which are due to wave elevation and non-uniform C_M (ref. Table II).

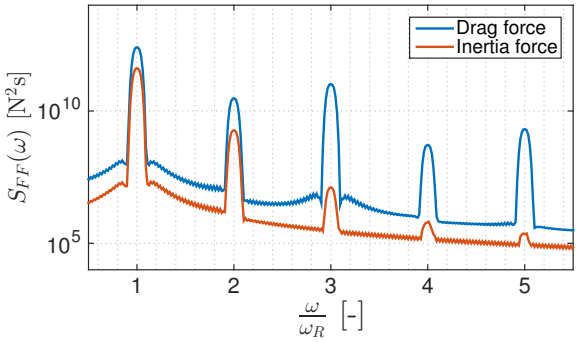

Fig. 4. Morison load on slender cylinder in regular waves with frequency ω_R. D=1[m]. Note logarithmic scale on y-axis.

B. Response

The wave load spectrum for the cylinder in Fig. 4 is reflected well in the resulting DAF for the base shear shown in Fig. 5. A multi-harmonic DAF function is fitted to the results using weight factors obtained analytically from eq. (10) with eq. (11). Note that $\sum_{n=1}^{N} k_n$ should be pre-defined. The damping ratios are adjusted to represent the peaks accurately.

$$k_n = \frac{|C_n|}{|C_1|} \cdot \frac{\sum_{n=1}^{N} k_n}{\sum_{n=1}^{N} |C_n|} \tag{11}$$

It is interesting to observe that the response at $\Omega = 0.33$ is larger than at $\Omega = 0.5$. This is partly due to an added damping from the harmonic terms in the drag load. To illustrate, a

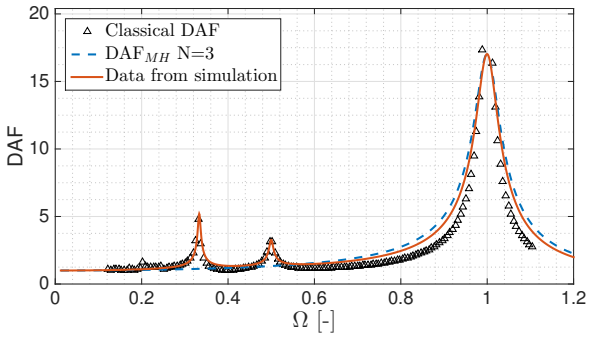

Fig. 5. Reaction moment DAF for slender cylinder in regular seas as a function of natural period. $\bar{k} = [0.87, 0.04, 0.09]$, $\bar{\zeta} = [0.021, 0.010, 0.011]$.

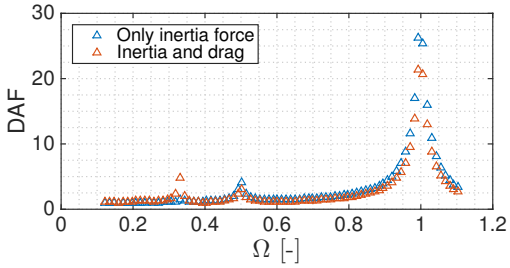

Fig. 6. Reaction moment DAF for slender cylinder in regular seas with and without drag force.

simulation is carried out with $C_D = 0$ meaning that only the inertia load is applied. Results are seen in Fig. 6, where a set-down of the DAF is observed at $\Omega = 1$ and 0.5. The inertia load is also somewhat non-linear due to wave elevation, as seen in Fig. 4, so a response peak is also observed at $\Omega = 0.5$.

C. Damping

The total damping can be expressed as a sum of several contributions. Here, ζ_s is used for the structural damping and there is no hydrodynamic damping. The additional damping, ζ_a, is then partly due to the multi-harmonic forcing on the cylinder.

$$\zeta_n = \zeta_s + \zeta_h + \zeta_{a,n} \tag{12}$$

If the responses at the resonant peaks are known, the additional damping can be found as approximately:

$$\zeta_{a,n} = \frac{k_n}{2\left(DAF_n - \sum_{j=1}^{n-1} DAF_{j,n}\right)} - \zeta_s \tag{13}$$

which is a simplified rearrangement of eq. (7) with respect to damping, where $\text{DAF}_{j,n}$ is the DAF at $\Omega = 1/n$ due to the harmonic load at $\Omega = 1/j$.

V. Efficient EDAF estimation

For regular waves, and hence regular response, there is no need for a collection of samples for statistical evaluation of DAF. EDAF on the other hand, requires several time-series, or seeds, to confidently evaluate a response level. The following subsection will address the topic of required amount of simulated data to accurately determine EDAF.

A. Method

Several methods to predict the q-probable response are presented in [13] and re-evaluated in [14]. In the latter, and in recent studies by the author, it is concluded that the Gumbel extreme value distribution, described in detail in [15], is the most stable and reliable. Therefore, it is the most widely used method in similar studies ([3], [7] and [16]). The Gumbel distribution is given in eq. (14),

$$F_Y(y) = \exp[-\exp[-\alpha(y-u)]] \tag{14}$$

where y represents the maximum value from each time-series. The parameters can be estimated from data, where σ is the standard deviation of the data, and μ is the mean.

$$\alpha = \frac{\pi}{\sqrt{6}\sigma} \tag{15a}$$

$$u = \mu - \frac{0.57722}{\alpha} \tag{15b}$$

However, there is a variation in the required number of 3 hour long simulations. At least 10 samples is recommended in [13], while 99 and 20 samples are used in [1] and [7], respectively. This is investigated in the next subsection.

Another promising method is the average upcrossing rate (AUR) used in e.g. [17] and [18]. In [16], it was shown that is gives a smaller confidence interval (CI) than the Gumbel method on a similar case. It is based on the assumption that the upcrossing events in the time-series are independent and Poisson distributed. This assumption is good for the largest responses in the time-series, which is verified in [19] for extreme wind speeds. The expression for the empirical AUR is given in eq. (16) for n number of upcrossings at level x, averaged over N time-series of length τ [s].

$$\hat{\nu}_x^+ = \frac{1}{N\tau}\sum_{i=1}^{N} n_i^+(x) \tag{16}$$

The results can be fitted to eq. (17) by the Levenberg-Marquardt least-squares algorithm.

$$\nu_x^+ = q(x)\exp(-a(x-b)^c) \tag{17}$$

Details can be found in [12] on weighting and estimation of empirical CI. It can be mentioned that the factor $q(x)$ can be approximated as a constant in the tail, and $c = 1$ corresponds to a Gumbel distribution.

B. Ensemble

A thorough investigation on the required number of samples in the ensemble is presented in Fig. 7 for extreme dynamic response. It is obtained with bootstrapping [20] at each seed to find the CI. Each vertical line represent 10 000 bootstrap samples. It is clear that 10 seeds is not sufficient, but 30 should be reasonable with the Gumbel method. The empirical CI using the AUR method is plotted alongside, indicating that it converges slightly faster.

VI. Response in irregular seas

The purpose of this section is to get an understanding of the response series that are dealt with in irregular seas for a dynamically sensitive structure.

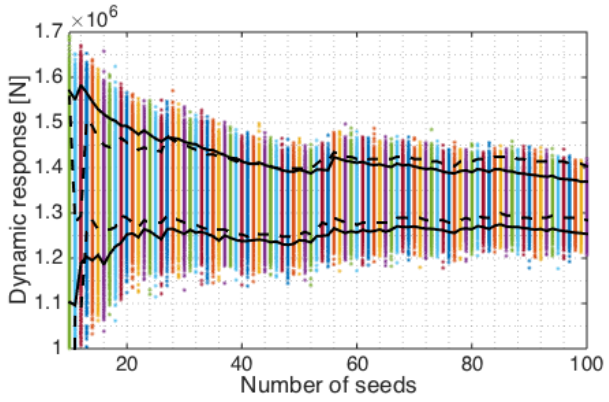

Fig. 7. Extreme dynamic response with Gumbel distribution at $\alpha = 0.9$, for the base shear of the slender cylinder. Black lines show the 95% CI. Dashed lines for AUR method.

A. Non-stationary, resonant response

The dynamic response for a structure can consist of several contributions. Fig. 8 shows an example where the jacket is subjected to irregular waves, and a resonant non-stationary response occurs after being subjected to several large waves. The response spectrum for this jacket with eigenperiod of 5[s] is shown in Fig. 9. For this eigenperiod, the resonant response

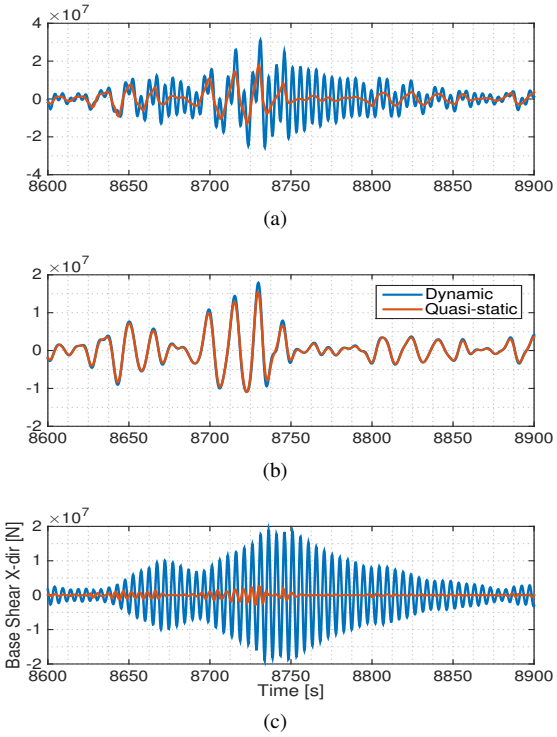

Fig. 8. Non-stationary response for jacket with $T_n = 5$[s]. Total response in (a), low-pass filtered in (b) and high-pass filtered in (c).

frequency is coinciding with the 3ω term from the drag load, resulting in large excitations. By evaluating the response series, it has been found that the dynamic extremes occur if 2 or more large waves follow each other. By contrast, the quasi-static response is only dependent on the single incident wave. From the response spectrum we can also observe that the peak

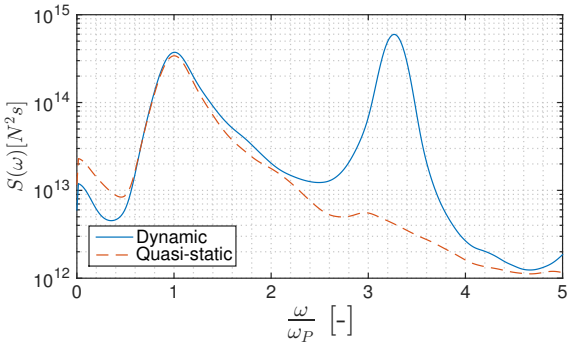

Fig. 9. Dynamic and quasi-static response spectrum in base shear for jacket with $T_n = 5$[s]. Averaged over 40 seeds and low-pass filtered.

loading period is $T = 0.97T_P$ in irregular seas, for the present case. This is due to a very narrow JONSWAP spectrum.

B. Correlation between dynamic and static extremes

As mentioned earlier, there is no guarantee that the extreme dynamic and quasi-static response will occur for the same wave incident. To illustrate this, the time-stamp of the extremes for 40 samples for the jacket with a natural period of 5 seconds are shown in Fig. 10 for reaction overturn moment. The correlation coefficient between the time-stamps is found to be in the range 0.22-0.28 for the reaction moment and 0.40-0.60 for the reaction base shear. This is explained by the fact that the base shear is directly related to the total wave load, in contrast to the reaction moment.

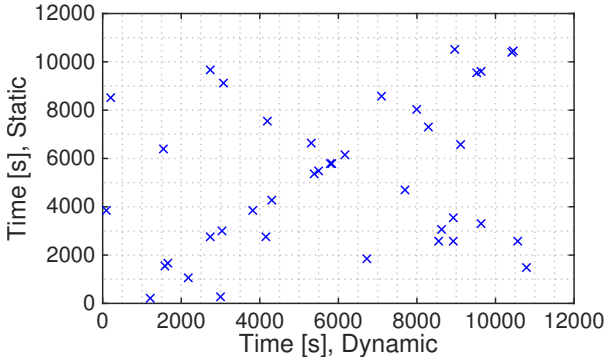

Fig. 10. Correlation between the time-stamp for occurrences of extreme reaction moment for jacket.

Also, there is some deviation in the relative magnitude of the responses. That is, a large dynamic response in a sample does not necessarily mean a large quasi-static response. This is illustrated in Fig. 11 for the same case as the figure above.

C. Uncertainty estimation

A confidence interval for EDAF can be obtained if the dependence between dynamic and static extremes is described. By investigating Fig. 11, we can find that there is a large probability that the quasi-static extreme is larger than the mean quasi-static extreme whenever the dynamic extreme is larger than the mean dynamic extreme (and vice versa). Therefore, one could say that always taking the mean static value is

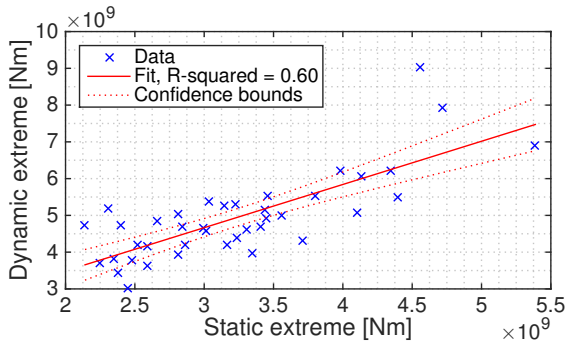

Fig. 11. Correlation of extremes between samples of reaction moment for jacket.

expected to be a conservative choice with respect to DAF. This method is adopted when the Gumbel and AUR fittings are used. The Gumbel values are bootstrapped to find a marginal distribution of the response at each fractile as shown in Fig. 12. Fig. 13 illustrates how the CI is obtained for the AUR method.

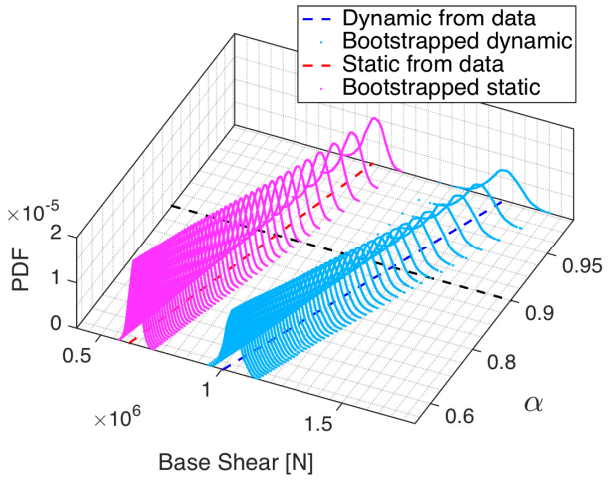

Fig. 12. Gumbel plot in with PDF of bootstrapped values for cylinder with 40 seeds. XY plane is the Gumbel probability paper. The 0.9 fractile level is marked with a dashed line.

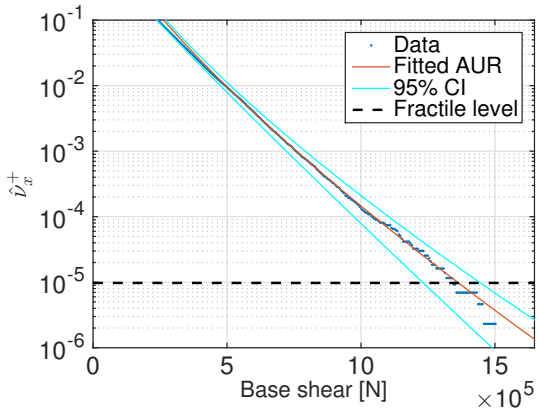

Fig. 13. AUR with CI for dynamic response of cylinder.

A second method is to find EDAF for each individual pair of dynamic and quasi-static seed. Then, a 3-parameter Weibull distribution (eq. (18)) is fitted to the local maxima in each time-series to obtain the q-probable extreme. This is done by a least-squares fitting with a weight towards the right tail to predict extremes more accurately. An example fit is shown in Fig. 14. And since only 30-40 seeds are used, the Weibull fittings are bootstrapped to obtain an accurate 95% CI.

$$F(x) = 1 - \exp\left[-\left(\frac{x-\gamma}{\sigma}\right)^{\beta}\right];\ \sigma, \beta, (x-\gamma) > 0 \quad (18)$$

The extreme values are found at a fractile of α =0.9 in the Gumbel plot for 3 hour simulations. This corresponds to the 30 hour characteristic extreme, and the percentile in a Weibull plot can be found with eq. (19), where τ is the simulation time and N_m is the number of local maxima (positive and negative). In this case $\hat{\alpha} = 0.99994$ since $\frac{\tau}{N_m} \approx 6.1$[s] ($\approx \frac{T}{2}$).

$$\hat{\alpha} = 1 - \frac{\tau}{N_m}\frac{1}{30\text{h}} \quad (19)$$

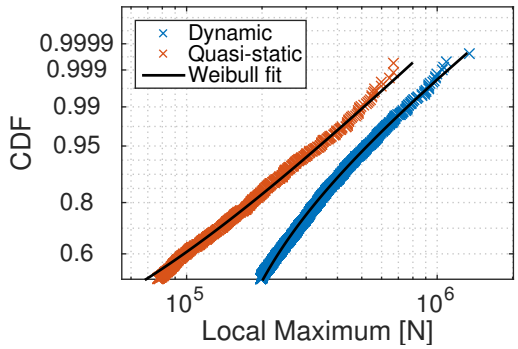

Fig. 14. 3-parameter Weibull distribution fitted to the tail of base shear response for cylinder.

VII. Results

A. Cylinder

The EDAF in irregular sea for the slender cylinder in shown in Fig. 15. The eigenperiod in the estimator is modified to account for damping and average load period, while added damping is deduced from the five visible peaks. Further, a MH DAF function with $\sum k_n = 1.1$ seems to fit reasonably well, since the curve is lifted to larger DAF values. It is also seen, that the harmonics at $\Omega = 0.25$ and 0.20 has to be accounted for to get a good fit. For the cylinder in Fig. 15, the Young's modulus (E [GPa]) is varied to obtain different natural periods. However, this leads to very large, unphysical displacements when $\Omega > 0.5$. It was observed a horizontal displacement of up to $0.3h$.

To avoid large displacements, a top-mass varied cylinder has been used instead. The DAF in irregular seas in shown in Fig. 16, and the results are similar for $\Omega < 0.5$. Note that the MH DAF function is not quite able to represent the response around $\Omega = 0.6$ in Fig. 16 for the stiff cylinder.

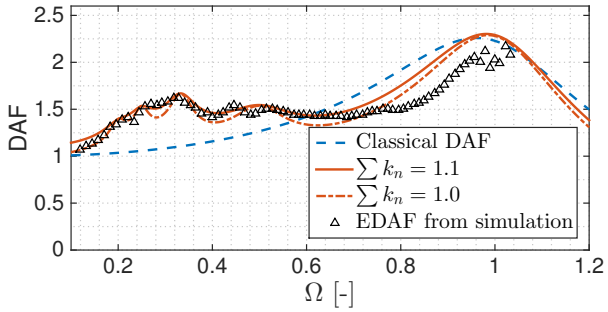

Fig. 15. DAF in base shear for cylinder with Gumbel distribution at $\alpha = 0.9$. Stiffness varied eigenperiod. $\bar{k} = [0.76, 0.14, 0.10, 0.05, 0.03]$, $\bar{\zeta} = [0.16, 0.14, 0.09, 0.08, 0.14]$

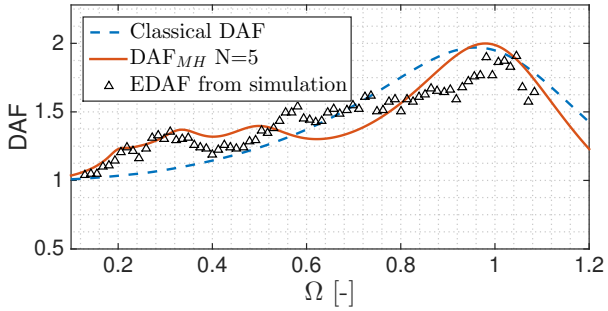

Fig. 16. DAF in base shear for cylinder with Gumbel distribution at $\alpha = 0.9$. Mass varied eigenperiod. $\bar{k} = [0.76, 0.14, 0.10, 0.05, 0.03]$, $\bar{\zeta} = [0.18, 0.16, 0.16, 0.22, 0.10]$

B. Jacket

The results for the jacket base shear and reaction moment are shown in Fig. 17 and 18, respectively. Fewer, but more realistic eigenperiods are simulated, with jackets and jack-ups in mind, but also due to large computational efforts compared to a single cylinder. As a guidance, $\Omega = 0.3$ corresponds to an eigenperiod of 4.6 [s], since $T_n \approx \Omega \cdot T_Z$.

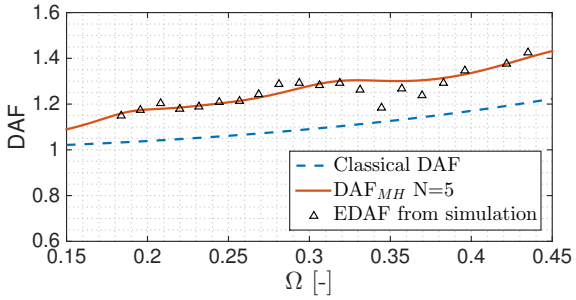

Fig. 17. DAF in base shear for jacket with Gumbel distribution at $\alpha = 0.9$. 32 seeds at each eigenperiod. $\bar{k} = [0.76, 0.14, 0.06, 0.03, 0.02]$, $\bar{\zeta} = [0.19, 0.16, 0.15, 0.20, 0.13]$

Results show that DAF for the jacket is in general slightly smaller than for the cylinder. This is most likely due to larger added damping as a result of cancellation of wave loading on many surface piercing braces and legs.

EDAF for the jacket reaction moment has been found using

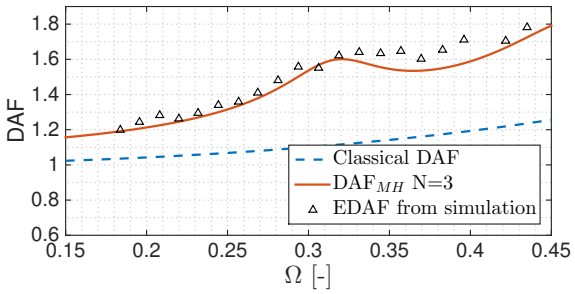

Fig. 18. DAF in reaction moment for jacket with Gumbel distribution at $\alpha = 0.9$. 32 seeds at each eigenperiod. $\bar{k} = [0.88, 0.15, 0.07]$, $\bar{\zeta} = [0.14, 0.11, 0.09]$

both the Gumbel and AUR method. A comparison is shown in Fig. 19, where is it clear that there are some differences around $\Omega = 0.33$. This is explained by the increased occurrence of resonant responses when the eigenperiod of the jacket is close to three times the load frequency. The AUR method will then extrapolate these responses, predicting up to 10% larger response than what is actually occurring in the tail. The Gumbel method on the other hand, does not recognize this behavior since it is only evaluating the absolute extreme response. Sticking to the definition of EDAF, the AUR method is too conservative when Ω is between 0.3 and 0.4.

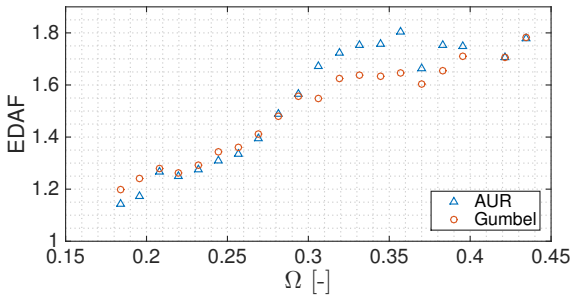

Fig. 19. Reaction moment EDAF for jacket in irregular waves.

C. Uncertainty estimation

With the three mentioned methods for finding a confidence interval, we obtain the CI in Fig. 20. Here, EDAF is plotted

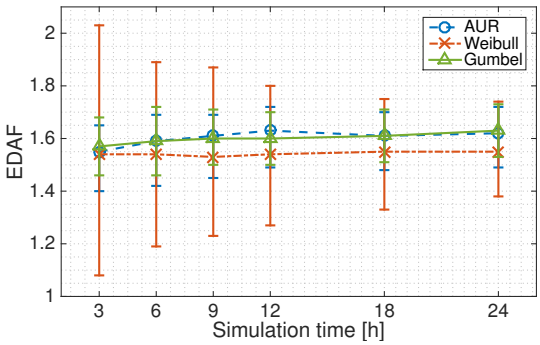

Fig. 20. EDAF with CI for cylinder with $T_n = 5.0$[s]. 40 seeds are used for each simulation time.

against continuous simulation time, which indicates that a large amount of data needs to be available for the Weibull method to approach the Gumbel and AUR results, which seems to be fairly stable when longer simulation time is accounted for.

The AUR and Gumbel estimated CI is shown in Fig. 21 for eigenperiod varied reaction moment for the jacket. The size of the CI is comparable to the CI for the cylinder in Fig. 20. It also seems that the empirical AUR CI estimates the upper bound for the CI closer to the expected EDAF.

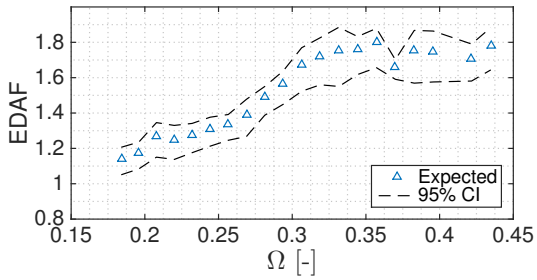

(a)

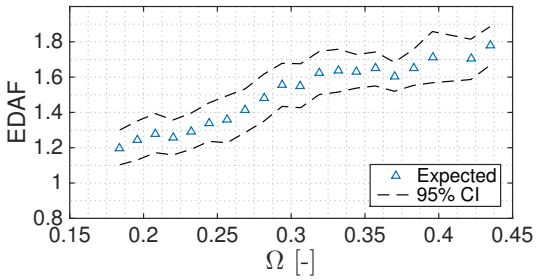

(b)

Fig. 21. Reaction moment EDAF with CI for AUR in (a) and Gumbel method in (b).

D. Damping coefficients

In Fig. 22, the weight factors and total damping coefficients for the cylinder and the jacket are plotted. Despite two very different structures, the fit is quite good. To verify this relationship, more drag dominated structures should be simulated in a similar manner. Also, different relations based on structure type would be preferable, but not done in this case. These curve fittings will form the basis for the case in the next subsection.

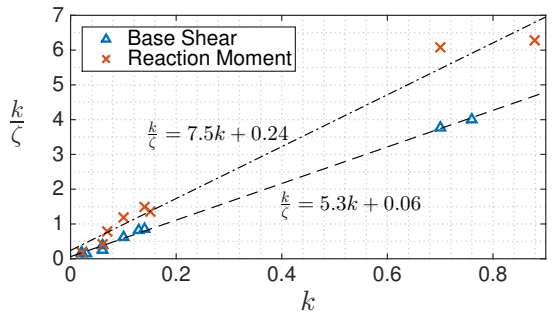

Fig. 22. Relation between weight factors (k) and damping ratios (ζ) for mass varied cylinder and jacket.

E. CASE

A small case study has been performed in order to determine if the multi-harmonic DAF function can be used to predict the dynamic response of a jack-up before full time-domain simulations are carried out. The jack-up in this case is an example jack-up located at a water depth of 110[m] and an air gap of 40[m]. The natural period is 7-8[s] during operation. It is subjected to full 3 hour simulations with the chosen sea-state and linear wave theory. The structural damping is the same as for the cylinder and jacket, about 1.5%. An illustration of the relatively complex model is shown in Fig. 23.

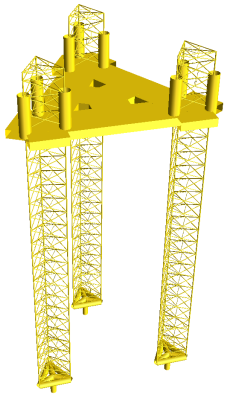

Fig. 23. Jack-up model in USFOS.

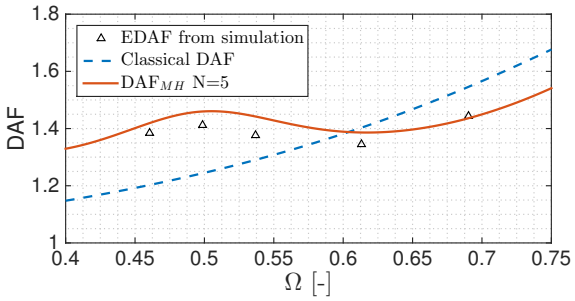

(a)

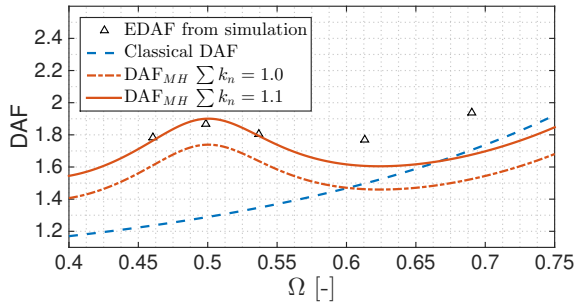

(b)

Fig. 24. DAF for jack-up case, with base shear in (a) and reaction moment in (b). 32 seeds for each case.

First, weight factors (k_n) are found after a wave load spectrum analysis. They were found to be: $\bar{k} = [0.73, 0.16, 0.06, 0.03, 0.01]$. The equations in Fig. 22 is then

used to find the total damping coefficients (ζ). The MH DAF line is then plotted, as seen in Fig. 24. Second, analysis are performed. Even though only linear wave theory are used, the detailed structure requires almost 12 CPU hours per 3 hour real-time simulation. For dynamic and quasi-static analysis with 30 seeds, this means 720 CPU hours, or nearly 4 days on a PC with 8 cores. In other words, a lot of computational efforts can be saved if an analytical formulation is available.

The final results are shown in Fig. 24 for five different eigenperiods. It is seen that the MH DAF function corresponds surprisingly well to the simulated results for base shear. The reaction moment deviates more for $\Omega > 0.6$, but the proposed DAF function is closer than the classical SDOF analogy. As seen in Fig. 24 (b), it is necessary to adjust the sum of the weight factors to get a more accurate result.

VIII. Conclusion

For full time-domain simulations, it has been shown that a large amount of data is required to estimate dynamic effects for a drag dominated structure in extreme, irregular seas. More specific, a minimum of 30 seeds for 3 hour analyses are needed if the Gumbel method is used. Slightly fewer seeds can be used for the AUR method. Both the Gumbel and AUR method are appropriate to estimate EDAF, but if the results seem to be well behaved in the tail, a Gumbel analysis is easier to implement and requires less post-processing. The Weibull method is too unstable to predict EDAF confidently.

The method of finding weight factors for the MH DAF function from the wave load spectrum is verified. The factors are quite similar for both the cylinder and the jacket, and close to what is used in [2]. The added damping coefficients however, are depending more on the response mode, reflecting excitation and cancellation frequencies. It is also confirmed that a drag dominated structure may experience a significant dynamic amplification at the 3ω load frequency. This is the most important effect for the investigated extreme sea-state. Results also show that the response at 2ω, 4ω and 5ω should be accounted for to approximate the simulated response. It is also interesting to see that good curves can be found without detailed knowledge of the damping at $\Omega = 1$ for a structure with $\Omega < 0.6$.

A conclusion is made that if reasonable damping coefficients are chosen, the multi-harmonic DAF function will give a good estimate for the actual DAF, both in regular and irregular waves. In regular waves, the total damping coefficients are fairly close to the structural damping when $\Omega \leq 0.5$, but much larger for irregular waves. Using an example jack-up, results from the fitted MH DAF function for the cylinder and jacket are put to the test. It does indeed show that an analytical formulation capturing multi-harmonic effects for a drag dominated structure is applicable. Taking into account the uncertainty in the EDAF estimate when simulating in irregular waves, the MH DAF function may give just as reliable results as full time-domain simulations. Also, further use of the classical SDOF DAF function should be discontinued for drag dominated structures.

Future analyses should include second order wave theory as the DAF is expected to increase due to ringing events caused by large, steep waves [3]. In addition, less severe sea-states could be simulated to investigate whether the same characteristics are present.

Acknowledgment

This work has been carried out at the Centre for Autonomous Marine Operations and Systems (AMOS). The Norwegian Research Council is acknowledged as the main sponsor of AMOS. This work was supported by the Research Council of Norway through the Centres of Excellence funding scheme, Project number 223254 - AMOS.

References

[1] D. Karunakaran, M. Baerheim, S. Haver, and N. Spidsoee, "Dynamic behaviour of Kvitebjørn jacket in north sea," in *Proceedings of the International Conference on Offshore Mechanics and Arctic Engineering - OMAE*, vol. 1, 2001, pp. 511–518.

[2] M. Williams, R. Thompson, and G. Houlsby, "Non-linear dynamic analysis of offshore jack-up units," *Computers & Structures*, vol. 69, no. 2, pp. 171–180, Oct. 1998.

[3] G. Baarholm, A. Johansen, J. Birknes, and S. Haver, "Estimation of equivalent dynamic amplification factor (EDAF) on a jacket structure," in *Proceedings of the International Conference on Offshore Mechanics and Arctic Engineering - OMAE*, vol. 1, Nantes, 2013.

[4] SINTEF and NTNU, "USFOS." [Online]. Available: http://www.usfos.no

[5] NORSOK, "N-003 Action and Action Effects." Standards Norway, 2007, no. September.

[6] S. R. Winterstein, T. C. Ude, C. A. Cornell, P. Bjerager, and S. Haver, "Environmental parameters for extreme response: Inverse FORM with omission factors," in *Proc. 6th Int. Conf. on Structural Safety and Reliability, Innsbruck, Austria*, 1993.

[7] S. Haver and S. R. Winterstein, "Environmental Contour Lines : A Method for Estimating Long Term Extremes by a Short Term Analysis," pp. 1–12, 2008.

[8] DNV GL, "RP-C205 Environmental conditions and environmental loads," Tech. Rep., 2010.

[9] M. Tucker, P. Challenor, and D. Carter, "Numerical simulation of a random sea: a common error and its effect upon wave group statistics," *Applied Ocean Research*, vol. 6, no. 2, pp. 118–122, Apr. 1984.

[10] ABS, "Guidance Notes on Dynamic Analysis Procedure for Self-Elevating Drilling Units," Tech. Rep. February, 2014.

[11] DNV GL, "RP-C104 Self-elevating Units," Tech. Rep. January, 2012.

[12] T. Moan and A. Naess, *Stochastic Dynamics of Marine Structures*. Cambridge University Press, 2013.

[13] SNAME, "T&RB 5-5a Recommended Practice for Site Specific Assessment of Mobile Jack-Up Units," Tech. Rep., 1994.

[14] X. Zhang, Z. Cheng, J. Wu, and C. Kei, "Dynamic response of jack-up units - Reevaluation of SNAME 5-5a four methods," in *Proceedings of the International Offshore and Polar Engineering Conference*, vol. 1, Beijing, 2010, pp. 357–362.

[15] E. Castillo, *Extreme value theory in engineering*, 1988.

[16] A. Naess, O. Gaidai, and S. Haver, "Efficient estimation of extreme response of drag-dominated offshore structures by Monte Carlo simulation," *Ocean Engineering*, vol. 34, no. 16, pp. 2188–2197, 2007.

[17] A. Naess, "Prediction of extremes of morison-type loading - An example of a general method," *Ocean Engineering*, vol. 10, no. 5, pp. 313–324, Jan. 1983.

[18] A. Naess and O. Gaidai, "Monte Carlo Methods for Estimating the Extreme Response of Dynamical Systems," *Journal of Engineering Mechanics*, vol. 134, no. 8, pp. 628–636, 2008.

[19] A. Naess and O. Karpa, "Statistics of bivariate extreme wind speeds by the ACER method," *Journal of Wind Engineering and Industrial Aerodynamics*, vol. 139, pp. 82–88, Apr. 2015.

[20] A. C. Davison and D. V. Hinkley, "Bootstrap Methods and Their Application," *Engineering*, vol. 42, no. 2, p. 216, 1997.